Journal of Materials Chemistry B

RSC Publishing

PAPER

Nanostructures based on monoolein or diolein and amphiphilic gadolinium complexes as MRI contrast agents†

Cite this: *J. Mater. Chem. B*, 2013, **1**, 617

Antonella Accardo,[a] Eliana Gianolio,[b] Francesca Arena,[b] Sabine Barnert,[c] Rolf Schubert,[c] Diego Tesauro[a] and Giancarlo Morelli*[a]

Highly ordered two or three dimensional mesophases in aqueous solution could be usefully obtained by using monoolein (MO) or diolein (DO) monomers. Nanostructures (also indicated as nanoparticles, NPs) of MO or DO containing different amounts (1%, 5%, 10% and 20%) of the synthetic amphiphilic gadolinium complex $(C18)_2$DTPA(Gd) have been prepared and characterized for their relaxometric and structural behaviors. The nanostructure is found in the 110–200 nm range for all investigated systems, while the presence of the gadolinium containing monomer produces a partial loss of the cubic symmetry, as shown by Cryo-TEM images of NPs doped with 10% w/w of $(C18)_2$DTPA(Gd). Gadolinium containing nanostructures display high relaxivity values (in the 10–15 mM^{-1} s^{-1} range at 25° and 20 MHz, with a further increase at 37 °C for DO based NPs), and interesting relaxometric properties for their possible use as MRI contrast agents. NPs containing 10% w/w of $(C18)_2$DTPA(Gd) (MO3-NPs and DO3-NPs) have been also derivatized by introducing 3% wt of $(C18)_2$–Peg_{3000}–FA to obtain targeted aggregates (MO3-NP–FA, DO3-NP–FA). A preferential uptake efficiency of DO3-NP–FA in IGROV-1 cells with respect to DO-NPs without folic acid is observed, especially when cells are incubated with low concentrations of nanostructures or at short incubation times, thus indicating its potential use as a target-selective delivery system for MRI contrast agents on tumor cells overexpressing the folate receptor.

Received 30th October 2012
Accepted 30th November 2012

DOI: 10.1039/c2tb00329e

www.rsc.org/MaterialsB

Introduction

Magnetic resonance imaging (MRI) contrast agents based on paramagnetic gadolinium complexes are widely used in biomedical research and clinical diagnosis.[1,2] They are essentially low molecular weight compounds that rapidly equilibrate between the intra and extravascular spaces after intravenous administration, improving MRI efficacy and providing physiological information along with the impressive anatomical details already obtained by magnetic resonance images without contrast.[3–5]

In order to obtain gadolinium based contrast agents with enhanced contrast efficacy and different pharmacokinetic properties, supramolecular aggregates, such as micelles and liposomes, containing Gd(III) complexes have been recently proposed as MRI contrast agents.[6–9] Liposomes are obtained by self-assembling aggregation of lipophilic gadolinium complexes, or by their co-aggregation with surfactants; micelles are based on amphiphilic poly(gadolinium complexes) polymers.[10] Moreover aggregates derivatized with bioactive molecules, such as peptides[8,11–15] and antibodies,[16–19] acting as target selective MRI contrast agents have also been recently proposed.

In addition to micellar and liposomal systems, amphiphilic molecules can display a variety of higher order two (2D) or three (3D) dimensional mesophases in aqueous solution. Phases such as the 2D inverse hexagonal or the 3D inverse cubic structures are attractive candidates for biomedical applications because they are thermodynamically stable in water and they can be dispersed as stable submicronal sized particles.[20] These mesophases contain extensive water channel networks and are under exploration as delivery systems of drugs or contrast agents. The nanostructures formed by dispersion of the bulk mesophases can offer substantial advantages with respect to traditional supramolecular aggregates; in fact they present: (a) much higher payloads of contrast agent ions compared to micellar and liposomal systems; (b) an expected increased relaxivity rate $(1/T_1)$, due to the slowing of the tumbling rate of the paramagnetic ions within the dense and highly ordered packing in the two and three dimensional networks of the hexagonal and cubic phases; (c) improved relaxivity values due to the presence of extensive nano-scale water channels that offer a better

[a]*CIRPeB, Department of Pharmacy & IBB CNR, University of Naples "Federico II", Via Mezzocannone, 16 80134 Napoli, Italy. E-mail: gmorelli@unina.it*

[b]*Department of Chemistry I.F.M. & Molecular Imaging Centre, University of Turin, Via Nizza, 52, 10125 Turin, Italy*

[c]*Department of Pharmaceutical Technology and Biopharmacy, University of Freiburg, Hermann-Herder-Str. 9, D-70104 Freiburg, Germany*

† The authors declare no competing financial interest.

environment for diffusion and fast exchange between gadolinium coordinated water and bulk water.

Contrast agents based on lanthanide complexes of oleates and phytanates[21–23] or on gadolinium and manganese complexes of EDTA derivatives of oleic and phytanyl acid,[24,25] in highly ordered two or three dimensional mesophases, have been recently proposed by Drummond *et al.*[21–25]

Here we report on the preparation, structural characterization and relaxometric behaviour of new gadolinium based contrast agents obtained by the co-aggregation of an amphiphilic gadolinium complex, $(C18)_2$DTPA(Gd), with molar excesses of monoolein (MO) or diolein (DO) (see Fig. 1). Monoolein and diolein are well known monomers used in the preparation of highly ordered two or three dimensional mesophases in aqueous solution. $(C18)_2$DTPA(Gd) contains the DTPA chelating agent which is well known to give thermodynamically stable and kinetically inert complexes with Gd(III) ions; moreover it shows interesting relaxometric properties both as self-assembled aggregates and in combination with amphiphilic peptides.[26]

Moreover, nanostructures derivatized with a new folate containing monomer (Fig. 1) have been studied by MRI and fluorescence with the aim to have target selective contrast agents for cells overexpressing the folate receptor.

Materials and methods

Materials

Protected N^{α}-Fmoc-amino acid derivatives, coupling reagents and Rink amide *p*-methylbenzhydrylamine MBHA resin were purchased from Calbiochem-Novabiochem (Laufelfingen, Switzerland). The DTPA$(OtBu)_4$–OH derivative was purchased from Chematech (Dijon, France). α-(9-Fluorenylmethyloxycarbonyl) amino-ω-carboxy poly(ethylene glycol) (Fmoc–NH–Peg_{3000}–COOH) was purchased from Iris Biotech GmbH (Marktredwitz, Germany). *N*,*N*-Dioctadecylsuccinamic acid was synthesized according to the literature.[27] Monoolein (1-monooleoyl glycerol, MO) and diolein (1,3-di(*cis*-9-octadecenoyl)glycerol, DO) were purchased from Sigma and had a purity of the acyl group (oleyl group) >99% and a purity of the ester (monoglyceride) >97%. A tri-block copolymer, containing ethylene oxide (EO) and propylene oxide (PO) groups, with the trade name Pluronic F127 (PF127) and an approximate formula of $EO_{98}PO_{57}EO_{98}$ (average molecular weight of 12 600 g mol^{-1}) was obtained from BASF Svenska AB (Helsingborg, Sweden). Rhod-PE (1,2-dioleoyl-*sn-glycero*-3-phosphoethanolamine-*N*-(lissamine rhodamine B sulfonyl) (ammonium salt)) was purchased from Avanti Polar Lipids (Alabaster, AL). All other chemicals were commercially available from Sigma-Aldrich,

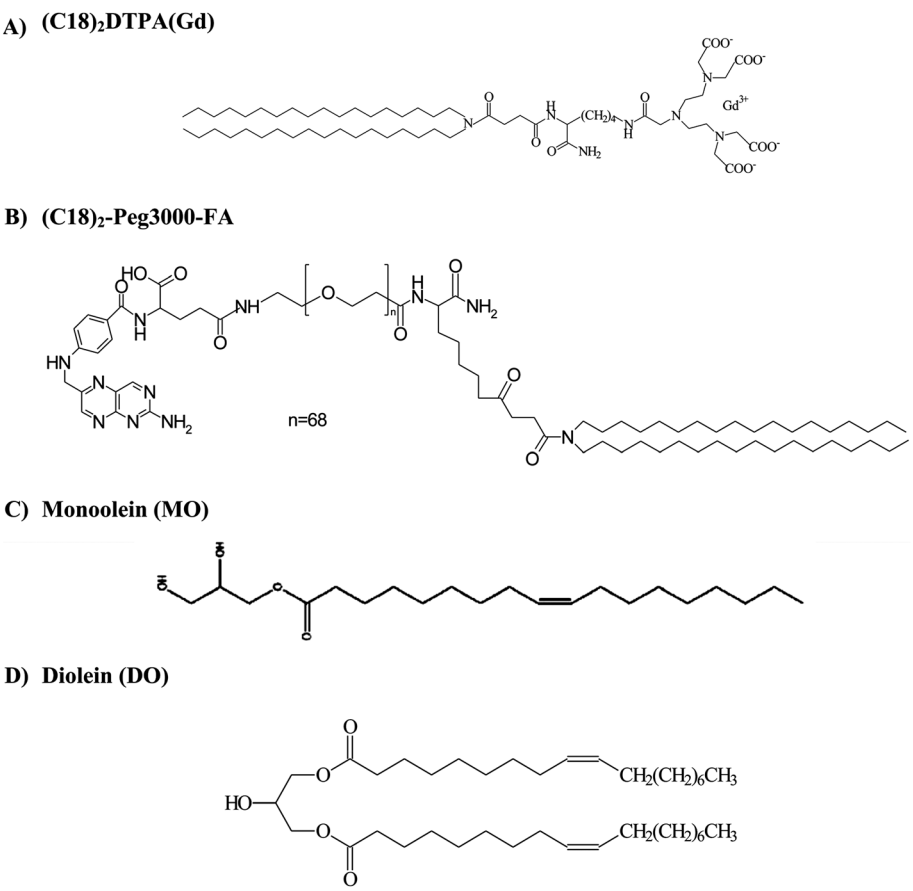

Fig. 1 Schematic representation of $(C_{18}H_{37})_2NCO(CH_2)_2COLys(DTPA\text{-}Gd)CONH_2$ [$(C18)_2$DTPA(Gd)] and $(C_{18}H_{37})_2NCO(CH_2)_2CO$–$Peg_{3000}$–folic acid [$(C18)_2$–$Peg_{3000}$–FA] monomers, and of the commercially available monoolein and diolein (MO and DO, respectively).

Fluka (Buchs, Switzerland) or LabScan (Stillorgan, Dublin, Ireland) and were used as received unless otherwise stated. All solutions were prepared by weight using doubly distilled water. The pH of all solutions was kept constant at 7.4. ^{1}H-NMR spectra were recorded by using a Varian 400 spectrometer (Palo Alto, CA USA). LC-MS analyses were performed by using a Finnigan Surveyor MSQ single quadrupole electrospray ionization (Finnigan/Thermo Electron Corporation San Jose, CA). UV measurements were performed on a UV-vis Jasco V-5505 spectrophotometer equipped with a Jasco ETC-505T Peltier temperature controller with a 1 cm quartz cuvette (Hellma).

Penicillin–streptomycin mixture, RPMI 1640, fetal bovine serum (FBS), and 0.25% (w/v) trypsin–0.03% (w/v) EDTA solution were purchased from Lonza (Lonza Sales AG, Verviers, Belgium). FFRPMI medium (modified RPMI 1640 medium without folic acid, vitamin B12 and phenol red) was obtained from Gibco BRL (MD, USA).

The human ovarian carcinoma cell line IGROV-1, human myeloid leukemia cell line K562, murine melanoma cell line B16-F10, and human epithelial cervical carcinoma cell line HeLa were obtained from American Type Culture Collection (Manassas, VA).

Chemical synthesis

$(C_{18}H_{37})_2NCO(CH_2)_2COLys(DTPA)CONH_2$, [$(C18)_2$DTPA], was synthesized by solid-phase methods and purified by precipitation or HPLC, as previously described.[26]

$(C_{18}H_{37})_2NCO(CH_2)_2CO$–poly(ethylene glycol)$_{3000}$–folic acid, $(C18)_2$–Peg_{3000}–FA, was obtained according to the following solid-phase procedure (Scheme 1). 0.374 g (0.60 mmol) of Dde–Lys(Fmoc)–OH activated by 1 equivalent of PyBop and HOBt and 2 equivalents of DIPEA in DMF were coupled twice to Rink-amide MBHA resin (0.51 mmol g^{-1}, 0.15 mmol scale, 0.295 g) by stirring the slurry suspension for 1 h. The solution was filtered and the resin was washed with three portions of DMF. The Fmoc protecting group was removed by two treatments with 2.0 mL of DMF–piperidine (70/30) mixture. After the Fmoc removal, *N*,*N*-dioctadecylsuccinamic acid was coupled using 4 equiv. (0.373 g, 0.60 mmol) of the lipophilic compound and HOBt/PyBop/DIPEA under standard conditions. Coupling reaction was carried out in 3 mL of DMF–DCM (50/50) for 1 h. The yield for aliphatic acid coupling, monitored by the Kaiser test, was in the range 95–98%. Thus Dde removal was performed by treatment of the resin with DMF–hydrazine (98/2). After Dde removal from the lysine residue, the Fmoc–Peg_{3000}–OH linker was coupled (2 equiv.) overnight by using HATU/DIPEA as activating agents and DMF as a solvent. Finally Fmoc from the polyethylene glycol linker was removed under standard conditions and then the folic acid (2 equivalents) was coupled at the N-terminus of the Peg moiety resin with a traditional coupling agent, HOBt–PyBop (2/2 equiv.), in DMF–DCM (50/50) and shaking the mixture for 5 h.[28] A small portion of the resin was removed for analysis. For deprotection and cleavage, the fully protected fragment was treated with TFA–H_2O (98/2). The crude product was precipitated at 0 °C, washed several times with small portions of water and recrystallized from methanol and water. The product was characterized by ^{1}H-NMR spectroscopy and electrospray spectrometry.

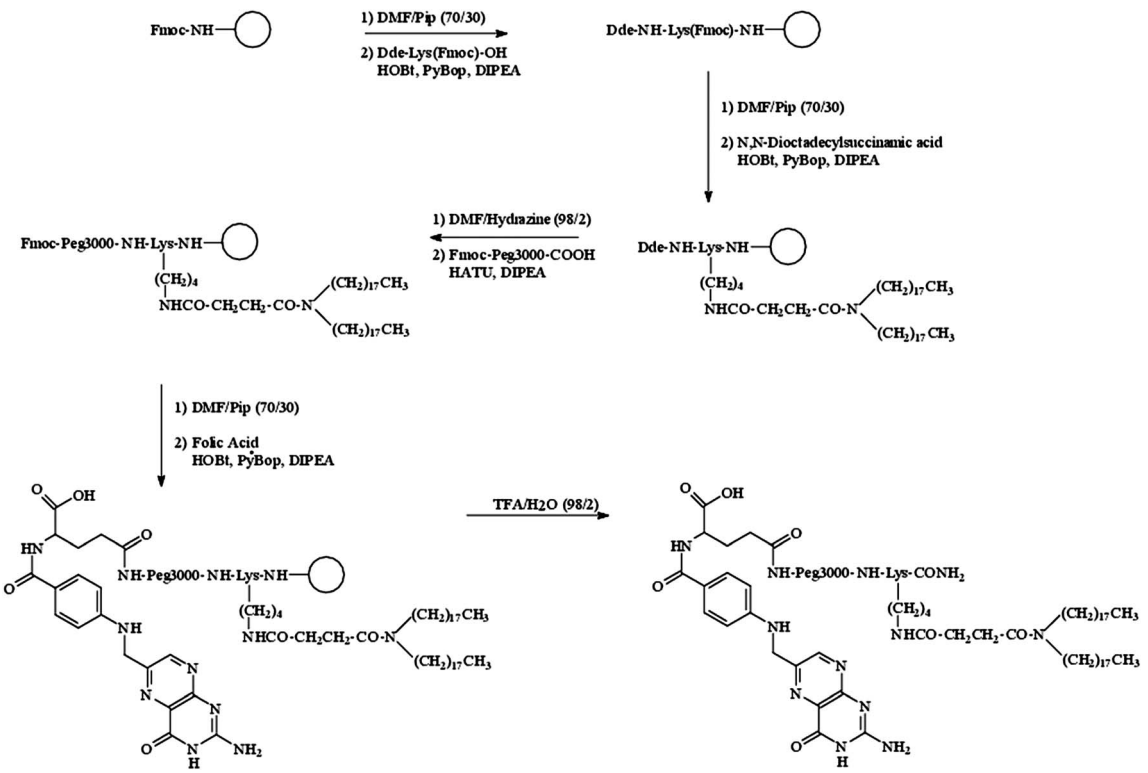

Scheme 1 Scheme for the solid-phase synthesis of the $(C18)_2$–Peg_{3000}–FA monomer. Rink-amide resin is schematically represented as an empty circle.

ESI MS = calc. 4135.5 amu; $[M + 3H^+]/3 = 1379.5$ amu; $[M + 4H^+]/4 = 1034.9$ amu.

^{1}H-NMR (400 MHz, DMSO d6): 8.75 (s, 1H), 7.64 (d, 2H), 6.74 (d, 2H), 4.52 (s, 2H), 4.3 (m, 1H, CH Lys α), 4.28 (dd, 1H), 3.60 (s, 270H), 3.1 (m, 2H, CH_2 Lys ε), 3.30–3.27 (m, 2H, N–CH_2), 2.8–2.4 (m, 6H), 2.1 (m, 2H), 1.90 (m, 2H, CH_2 Lys β), 1.6 (m, 2H, CH_2 Lys δ), 1.45 (m, 2H, CH_2 Lys γ), 1.27 (m, 60 CH_2 aliphatic), 0.89 (t, 6H, CH_3).

Synthesis and DLS analysis of nanostructures

Aqueous dispersions of MO or DO (MO-NPs and DO-NPs) containing various amounts of $(C18)_2$DTPA(Gd) amphiphilic gadolinium complex (1% ÷ 20%) were prepared by the method previously described.[4] Briefly, MO or DO, PF127, and $(C18)_2$DTPA(Gd) were weighed and mixed in chloroform. The weight ratio of PF127 to MO or DO was 15% (w/w). After evaporation of the solvent, the mixture was further dried in a vacuum. To the dry film was added 0.1 M phosphate-buffer at pH 7.4, and the vials were immediately sealed and vortexed for several seconds to distribute water inside the samples. The mixture was sonicated in a bath sonicator for 30 min and left overnight under stirring. Finally solutions were homogenized by using an ULTRA-TURRAX®(IKA® T18 basic) for 15 min in ice at 2.5 Hz. Targeted aggregates containing folic acid were prepared by introducing 3% wt of $(C18)_2$–Peg_{3000}–FA in the sample composition (MO3-NP–FA, DO3-NP–FA). The effective dimensions and surface charges of all MO-NPs and DO-NPs were measured by using a dynamic light scattering (DLS) instrument (Zetasizer-3000, Malvern Co., UK). The measurements were performed in phosphate-buffered saline solution (pH 7.4) and carried out in triplicate.

Relaxometric characterization of nanostructures

The proton $1/T_1$ NMRD profiles were measured over a continuum of magnetic field strength from 0.00024 to 0.47 T (corresponding to 0.01–20 MHz proton Larmor Frequency) on a Stelar Fast Field-Cycling relaxometer (Mede Pavia, Italy). This relaxometer works under complete computer control with an absolute uncertainty in $1/T_1$ of ±1%. Data points from 0.47 T (20 MHz) to 1.7 T (70 MHz) were added to the experimental NMRD profiles and were recorded on the Stelar Spinmaster spectrometer (Mede Pavia, Italy) with a switchable field from 20 to 70 MHz, by means of the standard inversion-recovery technique (16 experiments, 2 scans). A typical 90° pulse width was 4 μs and the reproducibility of the T_1 data was ±0.5%. The temperature was kept at 25 °C with a Stelar VTC-91 airflow heater (Mede Pavia, Italy) equipped with a copper-constant thermocouple (uncertainty ±0.1 °C). Relaxivity data at 20 MHz were measured on both instruments. Data were fitted to the conventional Solomon–Bloembergen–Morgan theory.

Cryo-TEM images

Cryo-TEM investigations were performed with a LEO 912 OMEGA electron microscope (Zeiss, Oberkochen, Germany) operating at 120 kV under 'zero-loss' conditions. After placing a droplet (approx. 5 μl) of the sample on a copper grid (Quantifoil® S7/2 Cu 400 mesh, holey carbon films, Quantifoil Micro Tools GmbH, Jena, Germany), most of the liquid was absorbed by a filter paper, so that only a thin (100–500 nm) liquid film remained. The sample was then immediately shock-frozen by plunging it into liquid ethane.[29] The vitrified sample was stored at 90 K in liquid nitrogen until it was loaded into a cryogenic sample holder (D626, Gatan Inc, Pleasanton, USA). The specimens were examined at −174 °C. Digital images were recorded with Proscan HSC 2 von Oxford instruments (Abingdon, USA), a "slow scan CCD camera system", and at minimal under-focus of the microscope objective lens to provide sufficient phase contrast.[30,31] Software: iTEM 5.0 (Build 1054), soft imaging System GmbH, Muenster, Germany.

In vitro cellular uptake

Different tumor cell lines (IGROV-1, B16-F10, HeLa, and K562) in FFRPMI (modified RPMI 1640 medium without folic acid, vitamin B12 and phenol red) were incubated with the same concentration of DO-NPs or DO-NP–FA for 4 h at 37 °C. After this incubation time, the cells were washed three times with 5 mL ice-cold phosphate-buffered saline (PBS), detached with EDTA and, for the acquisition of the MR images, collected in 50 μL of PBS, transferred into glass capillaries that were centrifuged at 1500*g* for 5 min and placed in an agar phantom. The MR-images were acquired by a standard T_1-weighted spin-echo sequence and recorded on an ASPECT M2 System operating at 1 T. At the end of MRI experiments labeled cells were quantitatively extracted from glass capillaries, dissolved in 2 mL of PBS and sonicated in order to destroy cellular membranes and obtain cell lysates. The Rhod-PE concentration was determined by measuring the emission peak at 594 nm (excitation at 543 nm) with a SpectroFluorometer (Fluoromax-4) and using a calibration line obtained using standard Rhod-PE solutions (1 nM ÷ 50 μM).

Then the solutions of labeled cells were freeze-dried and resuspended in 100 μL. These lysates were treated with 37% HCl (50 : 50) in sealed vials at 120 °C overnight. Upon this treatment all Gd^{3+} was solubilized as free aquo-ions. Then, the water proton $R_1(1/T_1)$ of these solutions was measured at 20 MHz and 25 °C on the Stelar Spin Master Relaxometer (Mede, Pavia, Italy), and the Gd^{3+} concentrations were determined from a calibration curve obtained using standard $GdCl_3$ solutions (0.01–2 mM).[32] The protein content was determined from cell lysates by the Bradford method using bovine serum albumin as the standard.[33] One mg of protein corresponds to 4.2×10^6, 6.3×10^6, and 4.5×10^6 of IGROV-1, B16-F10 and K562 cells, respectively.

Confocal analysis

Ca. 5×10^5 IGROV-1 (human ovarian adenocarcinoma cell lines) cells in a medium RPMI 1640 were incubated with 90 μL of Gd–DO-NPs (0.05 μM of [Rhod]) for 6 h at 37 °C. After this incubation time, the cells were washed three times with 5 mL ice-cold phosphate-buffered saline (PBS), and were fixed in 4% paraformaldehyde. Cell preparations were examined by

confocal laser scanning microscopy (Leica, Exton, PA SP5) with a 63 (0.90 numerical aperture) oil-immersion objective.

Results

Synthesis and structural characterization of nanostructures

Nanostructures (NPs) of MO or DO containing different amounts of $(C18)_2$DTPA(Gd) amphiphilic gadolinium complex (1%, 5%, 10% and 20%) were prepared and designed as MO1-NPs ÷ MO4-NPs or DO1-NPs ÷ DO4-NPs, respectively. Pluronic F127 in 15% w/w was also added to the nanostructure composition; this surfactant acts as a stabilizer of submicron particles with the bicontinuous cubic phase.[34] MO3- and DO3-nanostructures were also derivatized by introducing 3% wt of $(C18)_2$–Peg_{3000}–FA to obtain targeted aggregates (MO3-NP–FA, DO3-NP–FA). Fluorescent nanostructures were obtained by introducing 0.1% w/w of the fluorescent probe Rhod-PE for cellular studies. The effective composition of all studied nanostructures is indicated in Table 1.

Structural parameters (particle size and zeta potential) measured by DLS are reported in Tables 2 and 3. Concerning MO based nanostructures, the particle size remains in the expected range (diameter $\sim$ 170 nm) for samples containing lower amounts of $(C18)_2$DTPA(Gd) (MO1-NPs, MO2-NPs); in contrast a diameter reduction is observed for nanostructures containing higher amounts of gadolinium complex (MO3-NPs and MO4-NPs).[35] In contrast, the particle size of DO nanostructures (around 180 nm) is not affected by the amount of $(C18)_2$DTPA(Gd). The zeta potential values of all investigated nanostructures are negative, with values ranging between -25 and -73 mV, as expected for the presence of the anionic gadolinium complex of DTPA.

The addition of $(C18)_2$–Peg_{3000}–FA and/or Rhod-PE to both MO3- and DO3-nanostructures does not affect significantly their size and zeta potential (Table 3).

Cryo-TEM images of MO3-NPs, MO3-NP–FA, DO3-NPs and DO3-NP–FA are shown in Fig. 2. In all preparations, vesicles were found but with a tendency to form complex mesophases. Fig. 2A shows a typical picture of MO3-NPs, where vesicles tend to fuse into foamy mesophases. In Fig. 2B (DO3-NPs) the prevalent structures are coexisting vesicles and tubules. In Fig. 2C and D (MO3-NP–FA) vesicles, foamy particles and aggregates of spoon-like structures are visible. Fig. 2E (DO3-NP–FA) again shows predominantly larger foamy mesophases.

Relaxometric properties of nanostructures

The relaxivity values (r_{1p}), defined as the paramagnetic contribution to the observed relaxation rate normalized to 1 mM concentration of the paramagnetic probe, of MO- and DO-based

Table 1 Composition (weight/weight percentage and molar concentration) of nanostructures

Formulation	% w/w $(C18)_2$DTPA(Gd)	[MO]/ mmol kg^{-1}	[DO]/ mmol kg^{-1}	[$(C18)_2$DTPA(Gd)]/ mmol kg^{-1}	[$(C18)_2$–Peg_{3000}–FA]/ mmol kg^{-1}
MO1-NP	1%	51.4	—	0.16	—
MO2-NP	5%	54.8	—	0.83	—
MO3-NP	10%	50.3	—	1.58	—
MO4-NP	20%	46.2	—	3.21	—
DO1-NP	1%	—	32.3	0.16	—
DO2-NP	5%	—	31.2	0.80	—
DO3-NP	10%	—	29.6	1.60	—
DO4-NP	20%	—	25.5	3.11	—
MO3-NP–FA	10%	50.5	—	1.56	0.145
DO3-NP–FA	10%	—	29.4	1.61	0.145

Table 2 Structural parameters (particle size, polydispersity index, and zeta potential) measured by DLS, and relaxivities (per Gd(III) ion) of MO- and DO-based nanostructures containing different $(C18)_2$DTPA(Gd) percentages

Formulation	% w/w $(C18)_2$DTPA(Gd)	r_{1p}[a] (mM^{-1} s^{-1})	Particle size (nm)	Polydispersity index PDI	Z potential (mV)
MO1-NP	1%	10.92	171.45 ± 0.56	0.205 ± 0.035	−28.60 ± 0.32
MO2-NP	5%	10.51	163.75 ± 0.66	0.190 ± 0.033	−45.60 ± 0.28
MO3-NP	10%	10.40	111.25 ± 0.34	0.130 ± 0.025	−49.10 ± 0.30
MO4-NP	20%	11.12	119.15 ± 0.65	0.210 ± 0.018	−48.00 ± 0.35
DO1-NP	1%	13.17	184.45 ± 0.58	0.180 ± 0.025	−31.60 ± 0.31
DO2-NP	5%	12.71	173.21 ± 0.49	0.306 ± 0.020	−63.20 ± 0.21
DO3-NP	10%	12.85	173.42 ± 0.51	0.160 ± 0.026	−25.76 ± 0.36
DO4-NP	20%	14.33	198.25 ± 0.65	0.185 ± 0.032	−73.20 ± 0.21

[a] Relaxivities were measured by using a Stelar Spin master spectrometer at 20 MHz and room temperature.

nanostructures containing different amounts (1 ÷ 20%) of $(C18)_2$DTPA(Gd) were measured at 20 MHz and 298 K (Table 2). For both oleic systems, relaxivity values are quite similar to the different loading values, with a slight increase when the percentage of the Gd-complex is brought to 20% (Fig. 3a). On the other hand, when monoolein- and diolein-containing particles are compared, a significant difference (20–30%) in the respective relaxivity values is observed. A deeper understanding of the relaxometric processes behind this difference may be found in the analysis of the Nuclear Magnetic Relaxation Dispersion (NMRD) profiles in which the relaxivity of a given system is investigated as a function of the applied magnetic field in the range 0.01–70 MHz (Proton Larmor Frequency). Fig. 3b shows the NMRD profiles of MO4-NPs and DO4-NPs, both containing 20% $(C18)_2$DTPA(Gd), measured at 298 K and neutral pH. The NMRD profiles have been analyzed in terms of the available theory of paramagnetic relaxation,[36–38] and the main relaxometric parameters have been determined and are reported in Table 4.

The main difference in the two systems seems to rely on their reorientational correlation times (τ_R), being six times longer for DO4-NPs than for MO4-NPs. This behavior is likely related to a more compact insertion of the Gd-complex, which is functionalized with two aliphatic chains, in the mesophase scaffold when it is built by diolein lipids instead of monoolein ones.

Relaxivity values associated with diolein- and monoolein-containing systems were also investigated as a function of temperature in the range 298 ÷ 343 K at a fixed frequency of 20 MHz (Fig. 4). While the relaxivity of MO4-NPs decreases as the temperature is increased, and in the case of DO4-NPs a bell shaped profile is obtained. The experimental points have been interpolated by applying the same Solomon–Bloemergen–Morgan theory applied for the fitting of NMRD profiles, and taking into account the temperature dependence of the involved relaxation times. The analysis of NMRD profiles is the technique of choice for an accurate determination of τ_R associated with paramagnetic species.[39] Therefore, for the analysis of the relaxivity, temperature dependence τ_R has been fixed to the value determined from NMRD. A very good agreement from the two sets of independent measures has been obtained for the principal relaxometric parameters affecting the relaxivity of the systems considered (Table 3).

Unambiguously, the temperature dependence of the relaxivity associated with DO4-NPs indicates that, at 20 MHz and 298 K, the relaxivity of the paramagnetic adduct is significantly limited by τ_M. In fact, the initial observed increase of r_{1p}, as the temperature increases (in the range 298 ÷ 310 K), may be accounted for in terms of eqn (1) which shows that, when $T_{1M} < \tau_M$ (as occurs in the case of DO4-NPs which are endowed with a very long τ_R value), the inner-sphere contribution to the observed relaxivity increases as the exchange of the inner-sphere water molecule becomes faster:

$$r_{is} = \frac{qC}{55.6}\frac{1}{T_{1M} + \tau_M} \quad (1)$$

where C is the molar concentration of the Gd-complex, q is the number of inner sphere water molecules and T_{1M} is the relaxation time of the protons of the coordinated water molecule. In the second part of the curve (in the range 310 ÷ 333 K), the opposite condition ($T_{1M} > \tau_M$) is met, and, as T_{1M} has an inverse proportionality to τ_R, an increase of temperature causes its elongation and a consequent decrease in r_{1p}.[40]

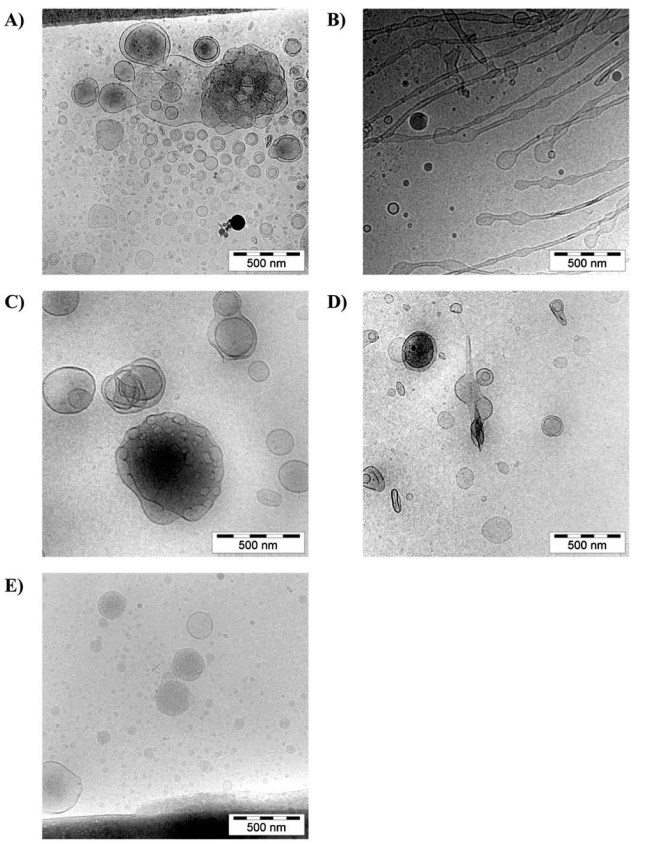

Fig. 2 Cryo-TEM images of nanostructures: (A) MO3-NP; (B) DO3-NP; (C), (D) MO3-NP–FA; and (E) DO3-NP–FA.

Table 3 Structural parameters (particle size, polydispersity index, and zeta potential) measured by DLS, and relaxivities (per Gd(III) ion) of MO- and DO-based nanostructures containing 10% $(C18)_2$DTPA(Gd), 0.1% Rhod-PE and 3% $(C18)_2$–Peg3000–FA

Formulation	r_{1p}[a] (mM^{-1} s^{-1})	Particle size (nm)	Polydispersity index PDI	Z potential (mV)
MO3-NP	10.40	111.25 ± 0.53	0.130 ± 0.020	−49.10 ± 0.32
MO3-NP–FA	10.00	150.45 ± 0.46	0.150 ± 0.030	−39.60 ± 0.28
DO3-NP	12.85	173.42 ± 0.88	0.160 ± 0.030	−25.76 ± 0.43
DO3-NP–FA	13.06	149.42 ± 0.44	0.120 ± 0.026	−27.76 ± 0.50

[a] Relaxivities were measured by using a Stelar Spin master spectrometer at 20 MHz and room temperature.

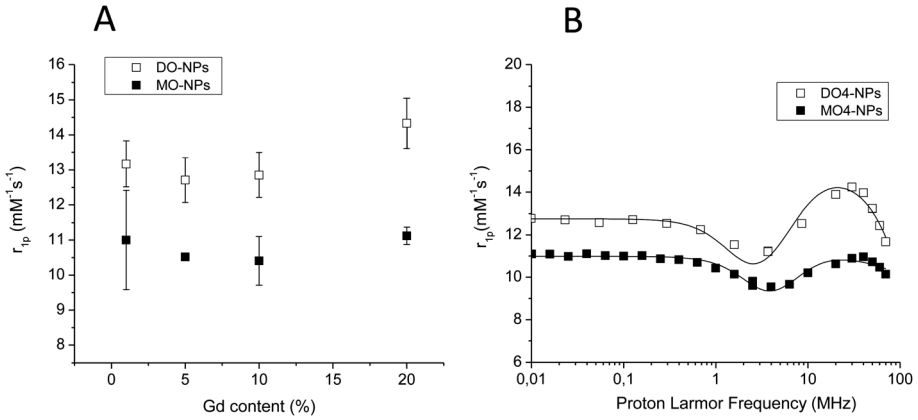

Fig. 3 (A) Proton longitudinal relaxivities of DO-NPs and MO-NPs, measured at 20 MHz and 298 K, as a function of different $(C18)_2$DTPA(Gd) loading extent. (B) Proton Nuclear Magnetic Relaxation dispersion profiles of MO4-NP and DO4-NP, containing 20% $(C18)_2$DTPA(Gd), measured at 298 K and neutral pH.

In Fig. 4 the effect of temperature on the relaxivity of MO4-NPs is also reported. The system shows an incipient limiting effect of τ_M only at low temperatures, whereas the overall decrease of r_{1p} *versus* T is a clear indication of a dominance of T_{1M} over τ_M in eqn (1).

The addition of Rhod-PE (0.1% wt) and $(C18)_2$–Peg_{3000}–FA (3% wt) to both MO- and DO-nanostructure preparations containing 10% $(C18)_2$DTPA(Gd) does not affect significantly their relaxivity values (Table 4).

In vitro cellular uptake

MO- and DO-NPs containing 10% $(C18)_2$DTPA(Gd) and doped with 0.1% of Rhod-PE have been functionalized for specific cell recognition through the insertion in the lipid composition of the amphiphilic folic acid containing molecules (MO3-NP–FA and DO3-NP–FA).

Folic acid, an oxidized form of folate, is an attractive targeting ligand due to its high binding affinity for the folate receptors ($K_d \sim 10^{-10}$ M) overexpressed on many tumor cells.

IGROV-1 cells, an ovarian cancer line which is known to possess an high expression of folate receptors,[41] have been incubated for 4 hours at 37 °C in FFRPMI (modified RPMI 1640 medium without folic acid, vitamin B12 and phenol red) with different concentrations (10–500 μM of Gd) of MO-NP–FA and DO-NP–FA as well as with the same concentrations of the unspecific MO-NPs and DO-NPs as a control. A further control experiment was carried out on a deficient folate-receptor cell line, B16-F10. Either MO-NPs or folate targeted MO-NPs (MO-NP–FA) resulted to be highly toxic for cells even at the lower concentration values (data not shown). Thus, for the following *in vitro* cellular experiments, only diolein-nanostructures were considered.

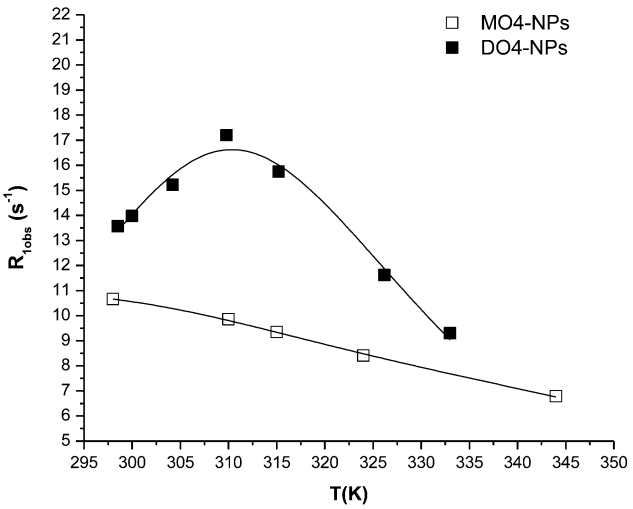

Fig. 4 Proton longitudinal relaxation rates of MO4-NPs and DO4-NPs ([Gd] = 0.9 mM) measured as a function of temperature at 20 MHz and neutral pH.

Cellular uptake was quantified by measuring either the Gd(III) or the rhodamine content normalized to 1 mg of protein in the cellular lysates (Fig. 5a and b). After the uptake time (4 h at 37 °C) cells were extensively washed, collected in phosphate-buffered saline (PBS) and sonicated to induce cell lysis. The

Table 4 Principal relaxometric parameters obtained from the fitting procedure of NMRD profiles shown in Fig. 3B and r_{1p} *vs.* T profiles shown in Fig. 4. In r_{1p} *vs.* T data analysis τ_R has been fixed to the values found from NMRD analysis

Samples	% $(C18)_2$ DTPA(Gd)	Δ^2 (s^{-2})		τ_V (ps)		τ_R (ps)	τ_M (μs)	
		NMRD	r_{1p} *vs.* T	NMRD	r_{1p} *vs.* T		NMRD	r_{1p} *vs.* T
MO4-NP	20%	$(1.44 \pm 0.08) \times 10^{19}$	$(1.01 \pm 0.22) \times 10^{19}$	42.1 ± 1.46	41.2 ± 1.33	580 ± 76	1.09 ± 0.13	1.16 ± 0.08
DO4-NP	20%	$(9.79 \pm 0.65) \times 10^{18}$	$(9.85 \pm 0.86) \times 10^{18}$	42.1 ± 1.27	41.9 ± 1.24	3470 ± 611	1.28 ± 0.019	1.42 ± 0.06

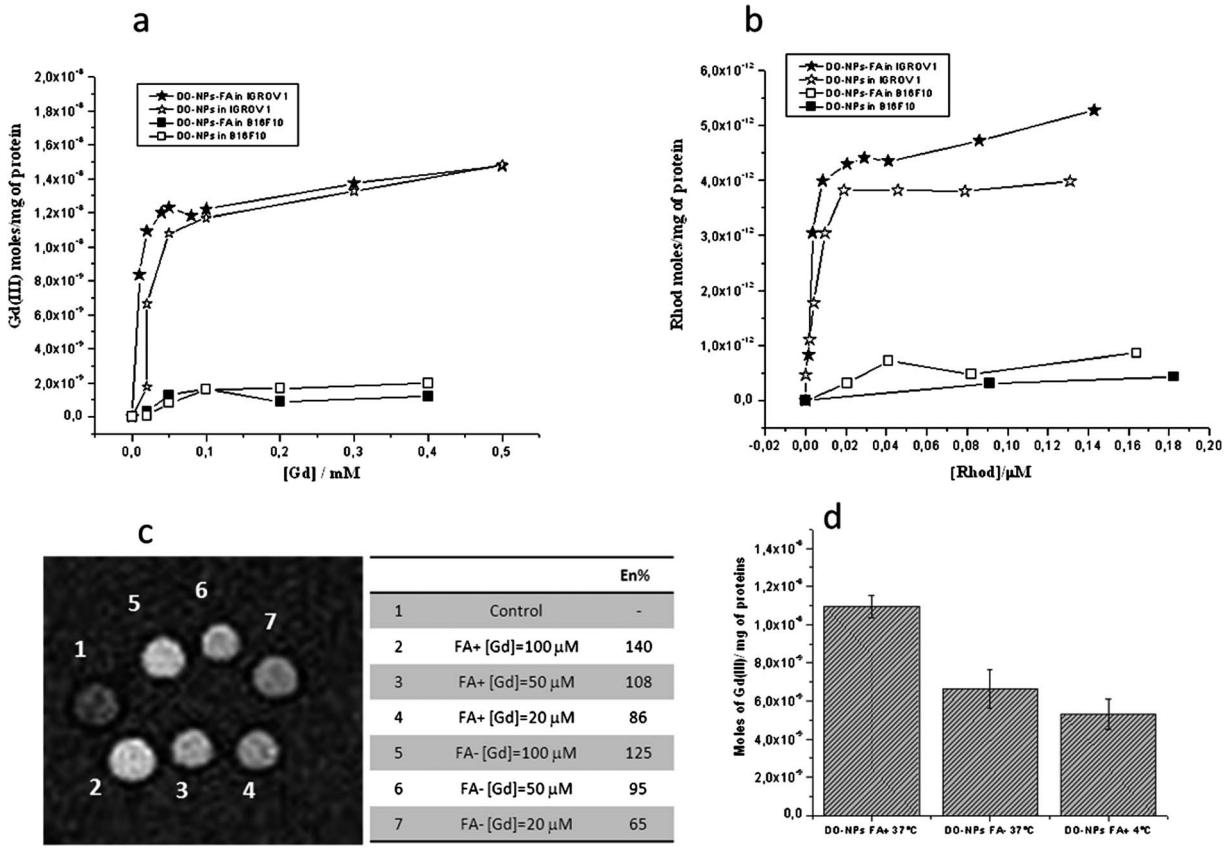

Fig. 5 Gd(III) (a) and Rhod-PE (b) contents of IGROV-1 (stars) and B16F10 (squares) cells measured through relaxometry and fluorescence respectively, after the incubation for 4 h at 37 °C with folic acid containing DO-NP–FA (black symbols) and DO-NPs without folic acid (white symbols); (c) T_1-weighted MR-image of a phantom containing IGROV-1 cells labeled with different concentrations (20–100 μM) of DO-NP–FA (2,3,4) and DO-NPs (5,6,7); (d) comparison of the amount of Gd(III) accumulated from IGROV-1 cells incubated with DO-NP–FA (Gd(III) concentration 20 μM) for 4 h at 37 °C and for 1 h at 4 °C. The amount of internalized Gd(III) with the same amount of DO-NPs without folic acid for 4 h at 37 °C is also reported.

Rhod concentration was determined by measuring the fluorescence emission peak at 594 nm. For the Gd(III) quantification, a relaxometric based method was used as reported in the Experimental section. We observed a high uptake level in IGROV-1 cells incubated with both targeted DO-NP–FA and not-targeted DO-NPs. Nevertheless, at low NP concentrations in the incubation media, uptake of folate-containing nanostructures resulted to be 15–40% higher than the corresponding one measured with non-targeted DO-NPs. Significantly lower internalization values were registered on B16-F10 control cells (Fig. 5a and b). The same behavior was observed by comparing the uptake in IGROV-1 cells with that measured in other tumor cells (K562, and HeLa) with low FA receptor expression (Fig. 6a and b).

An MRI investigation of IGROV-1 cells labeled with different amounts of DO-NP–FA and DO-NPs was carried out in the range of Gd(III) concentration 20–100 μM (Fig. 5c). In the T_1-weighted MR-image, labeled cells are markedly hyperintense with respect to the control unlabeled cells, with an enhancement factor dependent on the concentration of the paramagnetic probe in the incubation medium. The signal enhancement of labeled cells with respect to the control non-labeled ones has been calculated by using eqn (2):

$$\mathrm{En}(\%) = \frac{\mathrm{SI(NPs)} - \mathrm{SI(control)}}{\mathrm{SI(control)}} \times 100 \qquad (2)$$

Consistent with the cellular uptake shown in Fig. 5a, T_{1W} signal enhancements of cells labeled with DO-NP–FA are from 12% (for [Gd] = 100 μM) to 32% (for [Gd] = 20 μM) higher than the corresponding ones labeled with DO-NPs without folic acid. When active transport was blocked by conducting the uptake experiment at 4 °C (Fig. 5d) the amount of Gd(III) accumulated by cells was *ca.* 50% lower. This amount is similar, within the experimental error, to that found in cells incubated with non-targeted DO-NPs at 37 °C for 4 h.

Finally, a confocal microscopy analysis of IGROV-1 and B16-F10 cells incubated with Rhod-PE loaded DO3-NP–FA and DO3-NPs has been carried out (Fig. 7). The confocal images of IGROV-1 cells incubated with targeted NPs, when compared to those treated with untargeted NPs, show a higher fluorescence intensity at 2 hours of incubation while become similar after 4 hours of incubation. For both, but especially for the FA-containing nanostructures, the red fluorescence is localized on the external surface of cells indicating a binding to the cellular membrane but not a massive internalization of the probes.

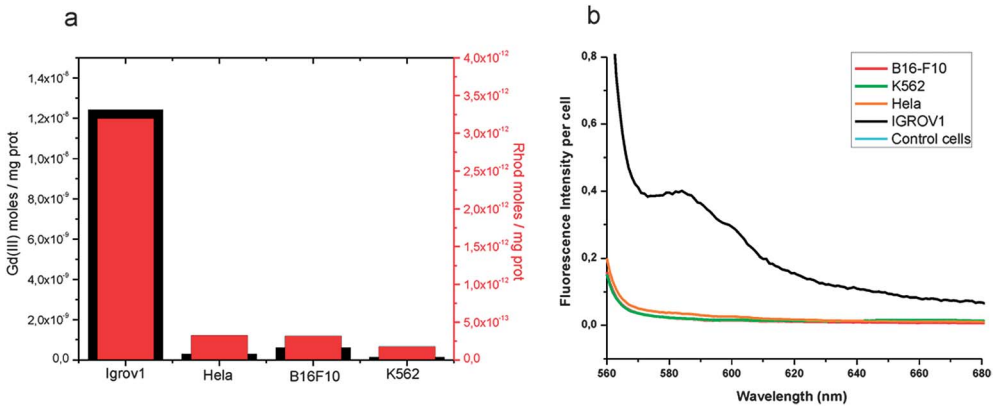

Fig. 6 (a) Gd(III) (black bars) and Rhod-PE (red bars) contents of IGROV-1, Hela, B16-F10 and K562 cells after incubation for 4 h at 37 °C with folic acid containing DO-NP–FA (Rhod-PE concentration 0.03 μM and Gd(III) concentration 50 μM). (b) Fluorescence emission spectra of cell lysates incubated for 4 h at 37 °C with DO-NP–FA (Rhod-PE concentration 0.03 μM) excited at 543 nm. The 594 nm peak corresponding to Rhod-PE emission is clearly visible only in the case of IGROV-1 cells.

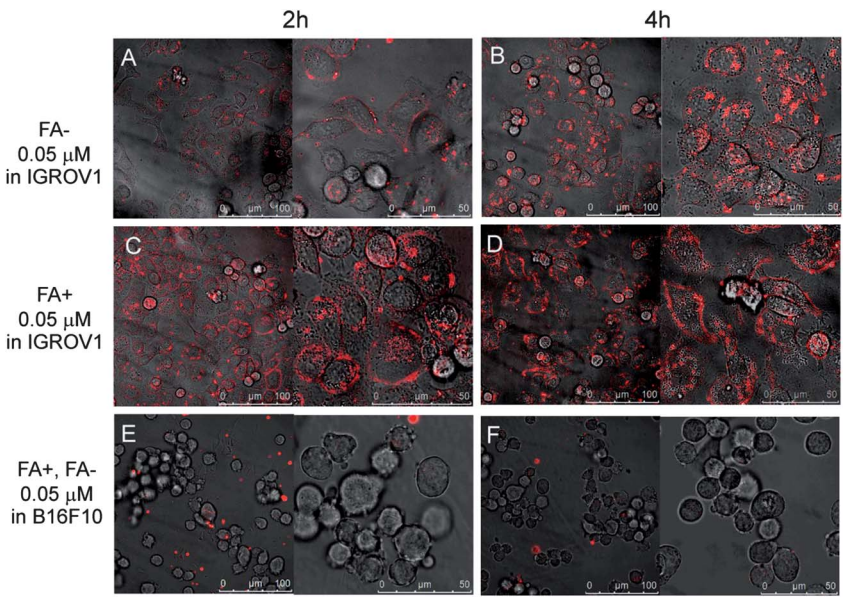

Fig. 7 Confocal microscopy analysis of IGROV-1 cells (A–D) incubated for 2 h (left) and 4 h (right) at 37 °C with DO-NPs (A and B) and DO-NP–FA (C and D) and B16F10 cells (E and F) incubated in the same time and temperature conditions with DO-NPs (E) and DO-NP–FA (F). For all the experiments the concentration of Rhod-PE is 0.05 μM.

On the other hand, consistent with cellular uptake results shown in Fig. 5b and in Fig. 6, any fluorescence signal was seen after 4 hours of incubation of the folate receptor deficient B16F10 cells incubated with either DO3-NP–FA or DO3-NP.

Discussion

Nonlamellar nanostructures are constituted by dispersion of self-assembled lipid mesophases corresponding to different non-lamellar phase structures such as reversed micellar cubic (I_{II}), reversed hexagonal (H_{II}), reversed bicontinuous cubic (Q_{II}) or "sponges" (L_3). Very few systems doped with chelated metal ions included in the cubic phase framework have been reported until now.[21–25,42] Examples have been reported in which the paramagnetic ion was included in the nanostructures through coordination to oleates or phytanates molecules leading to systems endowed with considerably low stability and relaxivity values.[21,26] An improvement from the stability point of view has been obtained for systems containing Gd(III) and Mn(II) ions complexed with EDTA-monoolein and diolein,[22] even if, in the case of Gd(III) doped systems, the thermodynamic and kinetic stability toward trans-metallation is not yet high enough to think of a possible *in vivo* application. Recently, cubic nanostructured lipid nanostructures doped with Ni(II)-EDTA-bis-oleoyl complexes have been characterized.[24,25]

It is known that highly ordered two or three dimensional mesophases in aqueous solution could be usefully obtained by using monoolein and diolein monomers. Anyway, as indicated by most of the reported cases, the cubic symmetry of the structure could decrease by increasing the percentage of the

metal doping (above 5% mol) and a mixture of uni- and bi-lamellar vesicles or liposomes can be observed.

Here we report on preparation, structural and relaxometric behavior, and *in vitro* binding studies of new gadolinium containing nanostructures. To the best of our knowledge, these are the first Gd-containing nanostructured systems displaying tendency to form complex mesophases, in which the Gd(III) metal ion is included in a thermodynamically stable complex. Different amounts of the amphiphilic gadolinium complex have been experienced in the nanostructure preparation (1 ÷ 20% wt). Moreover MRI nanostructures with potential selectivity towards the folate receptor (FR), overexpressed on many cancer types, were prepared by introducing a low amount (3% w/w) of an amphiphilic derivative of the folic acid ($(C18)_2$–Peg_{3000}–FA). As expected, doping of MO and DO nanostructures with 10% w/w of gadolinium containing monomer and/or 3% w/w of folic acid derivative produces a partial loss of cubic symmetry of the structure as indicated by Cryo-TEM images (Fig. 2) in which vesicles coexisting with tubules, foamy mesophases and spoon-like structures are well visible.

Relaxivity values associated with the different formulations of MO- and DO-nanostructures containing 1 to 20 % of $(C18)_2$DTPA(Gd) do not change in a significant way by changing the Gd(III)-complex content, and are quite close to the value (15.2 mM^{-1} s^{-1} at 20 MHz and 298 K) recently reported[26] for vesicles constituted by the same Gd-complex mixed with an octreotide-containing monomer ($(C18)_2$L5–Oct) in a 90 : 10 ratio. This result is indicative of a quite fast diffusion of water molecules inside the channels of the nanostructure framework which does not infer a kinetic limit on the observed relaxivity. By comparing MO- and DO-containing nanostructures, a difference in their relaxivity (20–30% higher in the case of DO-NPs) is observed. From the analysis of the NMRD (Nuclear Magnetic Relaxation Dispersion) profiles of the two systems, which allows a good estimation of the relaxation parameters governing a given paramagnetic system, it was found out that the main difference between the two systems seems to relay on the reorientational correlation times (τ_R) associated with the Gd-complex in the two lipid framework, being six times longer for DO4-NP than for MO4-NP. This behavior is likely related to a more solid and compact insertion of the Gd-complex, which is functionalized with two aliphatic chains, in the mesophase scaffold when it is built by diolein lipids instead of monoolein ones. The longer τ_R value associated with DO-NPs affects also the temperature dependence of its relaxivity (Fig. 4). In fact, while the relaxivity of MO4-NPs decreases as the temperature is increased, in the case of DO4-NPs a bell shaped profile is obtained with a further increase in the relaxivity, with respect to the value measured at 25 °C, which reaches a value of 17.0 mM^{-1} s^{-1} at 37 °C. Functionalization of MO- and DO-NPs with the amphiphilic folic acid containing molecule does not affect the relaxivity of the corresponding nanostructures (Table 3).

Folate based targeting, which allows a selective delivering of therapeutic and imaging probes to tumors,[43] has been extensively employed in nuclear medicine,[44] fluorescence imaging of cancer cells,[45] and MR-imaging by iron-oxide nanostructures[46] and by Gd-containing liposomes.[47] The folate receptor is overexpressed in many cancer types such as brain, kidney, lung, and breast cancers, and, in particular, in epithelial carcinomas such as ovarian cancer.[48] Folate targeted NPs, as well as the corresponding non-targeted ones, have been tested on IGROV-1 cells, an ovarian carcinoma cell line which has been proved to possess a very high level of α-FR expression.[41] At the concentration range used in the present study, MO-containing nanostructures resulted to be highly toxic for cells. This result is in agreement with literature data reporting that cubic phase dispersions based on glycerol–monoolein and different surfactants (at different lipid to polymer ratios) show massive hemolysis activity likely due to its high fusogenicity with respect to lipid mixing with cellular membranes. In contrast, it is known that glycerol–diolein based "sponges" show a very small degree of hemolytic activity (1–2%).[49] The hypothesis on the toxicity of monoolein based nanostructures stabilized with Pluronic F127 (PF127) is that they behave as a Trojan horse in which monoolein promotes bioadhesion and internalization of PF127 which, once inside the cells, may exert its toxic activity toward mitochondrial and nuclear membranes.[50] This could be the case also for MO-NPs in which PF127 is present as the stabilizer.

The uptake experiments were thus carried out only on DO-based nanostructures. IGROV-1 uptake efficiency of folate functionalized DO-NPs and folate free DO-NPs was assessed either by measuring the Gd(III) content or the rhodamine content in cell lysates. A preferential uptake efficiency of DO-NP–FA in IGROV-1 cells with respect to DO-NPs without folic acid was observed, especially when cells were incubated with low concentrations of nanostructures (Fig. 5) or at short incubation times (Fig. 7). Anyway, quite surprisingly, a very high labeling efficiency, in IGROV-1 cells, was found even with nanostructures lacking the folate vector (DO-NPs). The fluorescence intensity per cell measured on IGROV-1 cells labeled with DO-NP–FA is 20 times higher than that reported[47] for KB cells labelled with folate receptor-targeted bimodal fluorescent paramagnetic liposomes. It may be speculated that DO-NP–FA accumulation in IGROV-1 cells may be imputed to two distinct recognition pathways. On one side, the specific recognition of folate receptors overexpressed on IGROV-1 cells is exploited, and on the other side an accumulation occurs likely due to the presence of Pluronic F127 as the particle stabilizer. In fact, it has been reported that Pluronic-micelles[51] and Pluronic-adsorbed liposomes[52] are internalized by Caco-2 cells *via* clathrin-mediated and caveole-mediated endocytosis.

By comparing the uptake efficiency of DO-NP–FA and DO-NPs in other cell types with lower or no expression of folate receptors (B16F10, K562 and HeLa) we observed a drastic drop in Gd(III) and rhodamine contents. This behavior is easily explained in the case of DO-NP–FA, on the basis of the lack of uptake due to specific folate receptors recognition but remains unclear in the case of untargeted DO-NPs because the internalization mechanisms associated with the presence of Pluronic F127 should be potentially active on a wide range of cell lines.

Conclusions

Nanostructures based on monoolein and diolein, well known monomers used in the preparation of highly ordered two or three dimensional mesophases in aqueous solution, have been prepared and doped with different amounts of a synthetic amphiphilic gadolinium complex. Even if, as expected, the presence of the gadolinium containing monomer produces a partial loss of the cubic symmetry, gadolinium containing nanostructures display high relaxivity values and interesting relaxometric properties for their possible use as MRI contrast agents. This is particularly true in the case of diolein based nanostructures in which higher relaxivity values, with a further increase at 37 °C, are found, probably due to a more solid and compact insertion of the gadolinium complex in the mesophase scaffold built by diolein lipids.

Moreover gadolinium doped diolein NPs, derivatized on the external surface by folic acid-containing molecules, could act as a target-selective delivery system for MRI contrast agents. In fact, DO-NP–FA shows very low toxicity, with a degree of hemolytic effect below 2%, and preferential uptake efficiency in IGROV-1 cells expressing the folate receptor.

Abbreviations

DCM	Dichloromethane;
DIPEA	*N*,*N*-Diisopropylethylamine;
DMF	*N*,*N*-Dimethylformamide;
DTPA(tBu)$_4$-OH	Diethylenetriaminepentaacetate tetra-*tert*-butyl ester;
EDTA	Ethylendiaminetetraacetic acid;
Fmoc	9-Fluorenylmethoxycarbonyl;
HATU	*O*-(7-Azabenzotriazol-1-yl)-1,1,3,3-tetramethyluronium;
HOBt	1-Hydroxy-1,2,3-benzotriazole;
ICP	Inductively coupled plasma;
IGROV-1	Human ovarian adenocarcinoma cell lines;
MRI	Magnetic resonance imaging;
NMRD	Nuclear magnetic relaxation dispersion;
PyBOP	Benzotriazol-1-yloxytripyrrolidinophosphonium hexafluorophosphate;
Rhod-PE	1,2-Dioleoyl-*sn-glycero*-3-phosphoethanolamine-*N*-(lissamine rhodamine B sulfonyl) (ammonium salt);
TFA	Trifluoroacetic acid.

Acknowledgements

This work was supported by grants from the Italian Minister of Research (MIUR): Grant FIRB RBRN07BMCT, Grant PRIN E61J11000300001 and Grant PRIN 2009235JB7. The Italian Consortium CIRCMSB is also gratefully acknowledged.

References

1 I. R. Young, *Methods in Biomedical Magnetic Resonance Imaging and Spectroscopy*, John Wiley & Sons Ltd., Chichester, 2000.
2 P. A. Rinck, *Magnetic Resonance in Medicine*, ABW Wissenschaftsverlag GmbH, Berlin, 2003.
3 J. Li, D. Zheng, K. T. Bae, P. K. Woodard and E. M. Haacke, *Invest. Radiol.*, 1998, **33**, 578–586.
4 A. Mühler, *Invest. Radiol.*, 1998, **33**, 709–714.
5 A. Mühler, *MAGMA*, 1995, **3**, 21–33.
6 D. Delli Castelli, E. Gianolio, S. Geninatti Crich, E. Terreno and S. Aime, *Coord. Chem. Rev.*, 2008, **252**, 2424–2443.
7 W. J. M. Mulder, G. J. Strijkers, G. A. F. Van Tilborg, D. P. Cormode, Z. A. Fayad and K. Nicolay, *Acc. Chem. Res.*, 2009, **42**, 904–914.
8 A. Accardo, D. Tesauro, L. Aloj, C. Pedone and G. Morelli, *Coord. Chem. Rev.*, 2009, **253**(17–18), 2193–2213.
9 W. J. M. Mulder, G. J. Strijkers, G. A. F. van Tilborg, A. W. Griffioen and K. Nicolay, *NMR Biomed.*, 2006, **19**(1), 142–164.
10 D. Tesauro, A. Accardo, E. Gianolio, L. Paduano, J. Texeira, K. Schillen, S. Aime and G. Morelli, *ChemBioChem*, 2007, **8**, 950–955.
11 G. A. F. van Tilborg, W. J. M. Mulder, N. Deckers, G. Storm, C. P. M. Reutelingsperger, G. J. Strijkers and K. Nicolay, *Bioconjugate Chem.*, 2006, **17**, 741–749.
12 W. J. M. Mulder, D. W. J. van der Schaft, P. A. I. Hautvast, G. J. Strijkers, G. A. Koning, G. Storm, K. H. Mayo, A. W. Griffioen and K. Nicolay, *FASEB J.*, 2007, **21**(2), 378–383.
13 R. J. M. G. E. Brandwijk, W. J. M. Mulder, K. Nicolay, K. H. Mayo, V. L. J. L. Thijssen and A. W. Griffioen, *Bioconjugate Chem.*, 2007, **18**, 785–790.
14 M. Vaccaro, G. Mangiapia, L. Paduano, E. Gianolio, A. Accardo, D. Tesauro and G. Morelli, *ChemPhysChem*, 2007, **8**, 2526–2538.
15 A. Accardo, D. Tesauro, A. Morisco, G. Mangiapia, M. Vaccaro, E. Gianolio, R. K. Heenan, L. Paduano and G. Morelli, *JBIC, J. Biol. Inorg. Chem.*, 2009, **14**, 587–599.
16 W. J. M. Mulder, G. J. Strijkers, A. W. Griffioen, L. van Bloois, G. Molema, G. Storm, G. Koning and K. Nicolay, *Bioconjugate Chem.*, 2004, **15**, 799–806.
17 W. J. M. Mulder, G. J. Strijkers, K. C. Briley-Saebo, J. C. Frias, J. G. S. Aguinado, E. Vudic, V. Amirbekian, C. Tang, P. T. K. Chin, K. Nicolay and Z. A. Fayad, *Magn. Reson. Med.*, 2007, **58**(6), 1164–1170.
18 M. J. Lipinski, V. Amirbekian, J. C. Frias, J. G. S. Aguinado, V. Mani, K. C. Briley-Saebo, V. Fuster, J. T. Fallon, E. A. Fisher and Z. A. Fayad, *Magn. Reson. Med.*, 2006, **56**(3), 601–610.
19 V. Amirbekian, M. J. Lipinski, K. C. Briley-Saebo, S. Amirbekian, J. G. S. Aguinado, D. B. Weinreb, E. Vucic, J. C. Frias, F. Hyafil, V. Mani, E. A. Fisher and Z. A. Fayad, *Proc. Natl. Acad. Sci. U. S. A.*, 2007, **104**(3), 961–966.
20 A. Yaghmur and O. Glatter, *Adv. Colloid Interface Sci.*, 2009, **147–148**, 333–342.

21 G. Liu, C. E. Conn, L. J. Waddington, S. T. Mudie and C. J. Drummond, *Langmuir*, 2010, **26**(4), 2383–2391.
22 G. Liu, C. E. Conn and C. J. Drummond, *J. Phys. Chem. B*, 2009, **113**, 15949–15959.
23 C. E. Conn, V. Panchagnula, A. Weerawardena, L. J. Waddington, D. F. Kennedy and C. J. Drummond, *Langmuir*, 2010, **26**(9), 6240–6249.
24 M. J. Moghaddam, L. de Campo, L. J. Waddington, A. Weerawardena, N. Kirby and C. J. Drummond, *Soft Matter*, 2011, **7**, 10994–11005.
25 M. J. Moghaddam, L. de Campo, L. J. Waddington and C. J. Drummond, *Soft Matter*, 2010, **6**, 5915–5929.
26 A. Accardo, A. Morisco, E. Gianolio, D. Tesauro, G. Mangiapia, A. Radulescu, A. Brandte and G. Morelli, *J. Pept. Sci.*, 2011, **17**, 154–162.
27 L. Schmitt, C. Dietrich and R. Tampe, *J. Am. Chem. Soc.*, 1994, **116**, 8485–8491.
28 S. K. Sharma and J. W. Lown, *Tetrahedron Lett.*, 2002, **43**, 6665–6667.
29 J. Dubochet, M. Adrian, J. J. Chang, J. C. Homo, J. Lepault, A. W. McDowall and P. Schultz, *Q. Rev. Biophys.*, 1988, **21**, 129–228.
30 Y. Talmon, *Ber. Bunsenges. Phys. Chem.*, 1996, **100**, 364–372.
31 A. Rank, S. Hauschild, S. Förster and R. Schubert, *Langmuir*, 2009, **25**, 1337–1344.
32 F. Arena, B. S. Jebasingh, E. Gianolio, R. Stefania and S. Aime, *Bioconjugate Chem.*, 2011, **22**, 2625–2635.
33 M. M. Bradford, *Anal. Biochem.*, 1976, **72**, 248–254.
34 J. Gustafsson, H. Ljusberg-Wahren, M. Almgren and K. Larsson, *Langmuir*, 1997, **13**, 6964–6971.
35 P. T. Spicer, K. L. Hayden, M. L. Lynch, A. Ofori-Boateng and J. L. Burns, *Langmuir*, 2001, **17**(13), 5748–5756.
36 I. Solomon, *Phys. Rev.*, 1955, **99**, 559–565.
37 N. Bloembergen, *J. Chem. Phys.*, 1957, **27**, 572–573.
38 N. Bloembergen and L. O. Morgan, *J. Chem. Phys.*, 1961, **34**, 842–850.
39 S. Aime, M. Botta, M. Fasano and E. Terreno, *The Chemistry of Contrast Agents in Medical Magnetic Resonance Imaging*, ed. A. E. Merbach and E. Toth, John Wiley & Sons LTD, 2001, p. 5.
40 I. Bertini and C. Luchinat, *Coord. Chem. Rev.*, 1996, **50**, 1–300.
41 N. Kamaly, T. Kalber, M. Thanaou, D. J. Bell and A. D. Miller, *Bioconjugate Chem.*, 2009, **20**, 648–655.
42 G. Mangiapia, M. Vaccaro, G. D'Errico, H. Frielinghaus, A. Radulescu, V. Pipich, A. M. Carnerup and L. Paduano, *Soft Matter*, 2011, **7**, 10577–10580.
43 A. R. Hilgenbrik and P. S. Low, *J. Pharm. Sci.*, 2005, **94**, 2135–2142.
44 E. I. Sega and P. S. Low, *Cancer Metastasis Rev.*, 2008, **27**, 655–664.
45 I. B. Kim, H. Shin, A. L. Garcia and U. H. F. Bunz, *Bioconjugate Chem.*, 2007, **18**, 815–820.
46 H. Choi, S. R. Choi, R. Zhou, H. F. Kung and I. W. Chen, *Acad. Radiol.*, 2004, **11**, 996–1004.
47 N. Ding, Y. Lu, R. Lee, C. Yang, L. Huang, J. Liu and G. Xiang, *Int. J. Nanomed.*, 2011, **6**, 2513–2520.
48 P. S. Low, W. A. Henne and D. D. Doorneweerd, *Acc. Chem. Res.*, 2008, **41**, 120–129.
49 J. Barauskas, C. Cervin, M. Jankunenc, M. Spandyreva, K. Ribokaite, F. Tiberg and M. Johnsson, *Int. J. Pharm.*, 2010, **391**, 284–291.
50 S. Murgia, A. M. Falchi, M. Mano, S. Lampis, R. Angius, A. M. Carnerup, J. Schmidt, G. Diaz, M. Giacca, Y. Talmon and M. Monduzzi, *J. Phys. Chem. B*, 2010, **114**, 3518–3525.
51 G. Sahay, E. V. Batrakova and A. V. Kabanov, *Bioconjugate Chem.*, 2008, **19**, 2023–2029.
52 X. Li, D. Chen, C. Le, C. Zhu, Y. Gang, L. Hovgaard and M. Yang, *Int. J. Nanomed.*, 2011, **6**, 3151–3162.

